An Assessment of Fission Product Scrubbing in Sodium Pools Following a Core Damage Event in a Sodium Cooled Fast Reactor

M. Bucknor[1], M. Farmer[1], D. Grabaskas[1]

[1]Argonne National Laboratory, Argonne, Illinois, USA

E-mail contact of main author: mbucknor@anl.gov

Abstract. The U.S. Nuclear Regulatory Commission has stated that mechanistic source term (MST) calculations are expected to be required as part of the advanced reactor licensing process. A recent study by Argonne National Laboratory has concluded that fission product scrubbing in sodium pools is an important aspect of an MST calculation for a sodium-cooled fast reactor (SFR). To model the phenomena associated with sodium pool scrubbing, a computational tool, developed as part of the Integral Fast Reactor (IFR) program, was utilized in an MST trial calculation. This tool was developed by applying classical theories of aerosol scrubbing to the decontamination of gases produced as a result of postulated fuel pin failures during an SFR accident scenario. The model currently considers aerosol capture by Brownian diffusion, inertial deposition, and gravitational sedimentation. The effects of sodium vapour condensation on aerosol scrubbing are also treated. This paper provides details of the individual scrubbing mechanisms utilized in the IFR code as well as results from a trial mechanistic source term assessment led by Argonne National Laboratory in 2016.

Key Words: Sodium Fast Reactor, Source Term, Fission Product Scrubbing, Safety Analysis

1. Introduction

Mechanistic assessments of radionuclide release during postulated accidents at advanced reactor sites has repeatedly been referenced by the U.S. Nuclear Regulatory Commission as being expected to be included in any advanced reactor license application [1][2][3]. As part of a trial mechanistic source term (MST) assessment for a metal-fuelled, pool-type sodium-cooled fast reactor (SFR) [4], led by Argonne National Laboratory, a fission product scrubbing in sodium pools computational tool was utilized to estimate the quantity of fission product aerosols retained in the sodium pool during accident scenarios. The computational tool was originally developed during the Integral Fast Reactor (IFR) program and applies classical theories of aerosol scrubbing to the decontamination of gases produced as a result of fuel pin failures in an SFR. This paper provides an overview of the modelling approach utilized in the IFR pool scrubbing code along with results of fission product scrubbing from the trial mechanistic source term assessment [4].

2. IFR Pool Scrubbing Code Model Description

The modelling approach employed in the IFR pool scrubbing code was to utilize classical theories for pool scrubbing [5] where it is assumed that aerosol trapping occurs through particle deposition within isolated bubbles ascending through a liquid pool. Thus, detailed hydrodynamic phenomena such as jet (or plume) flow, bubble agglomeration, bubble shattering, bubble swarms, etc., are not addressed. Detailed models that attempt to incorporate these effects (at least for water pools) are provided elsewhere [6][7][8]. The approach used in the IFR code assumed a bubbly flow regime (i.e. isolated bubbles ascending through the pool

with a well-characterized terminal rise velocity) where the initial bubble size was limited by hydrodynamic [9] instability.

In terms of the overall accident sequence, the present model addresses fission product scrubbing during the early phase of the accident (i.e., a timescale which is not significantly larger than the bubble residence time in the pool). Thus, the model does not address long-term fission product retention in the sodium pool, which is determined by the gas-liquid equilibrium partition coefficients for the volatile fission product species. Studies in this area have been fairly extensive. A general literature review is provided by Castleman [10]. Equilibrium partition coefficients for cesium, iodine, and tellurium between liquid sodium and the gas phase have been measured by Haga et al. [11].

The code considers aerosol removal by the mechanisms of Brownian diffusion, inertial deposition, and gravitational sedimentation. In addition, the code accounts for the effects of sodium vapour condensation on aerosol trapping. The code does not treat aerosol removal by the mechanisms of thermophoresis [12] or diffusiophoresis [7], nor does it address the effects of particle growth by coagulation and/or sorption on the overall aerosol removal rate. Finally, the code is currently limited to the treatment of discrete aerosol particulate; i.e. the decontamination of volatile gaseous fission products via vapour-phase condensation is not addressed. It should be noted that unless otherwise specified, SI units are assumed for all quantities discussed in this paper.

2.1. Aerosol Transport Equations

The principal objective of the aerosol transport analysis is to calculate the pool decontamination factor (DF), which is defined as the ratio of the aerosol mass entering the pool to the aerosol mass exiting the pool, i.e.

$$DF = \frac{Aerosol\ mass\ entering\ the\ sodium\ pool}{Aerosol\ mass\ exiting\ the\ sodium\ pool}. \tag{1}$$

As previously mentioned, the current code addresses aerosol removal by the mechanisms of Brownian diffusion, inertial deposition, gravitational sedimentation, and vapour condensation only. For a given aerosol particle diameter, d_a, the differential equation governing the rate of aerosol removal from the bubble for the j-th removal mechanism is of the form:

$$\left(\frac{dn}{dz}\right)_j = -\alpha_j\, n\,, \tag{2}$$

where

$n =$ number of particles in the bubble with diameter d_a,

$z =$ coordinate parallel to the direction of the bubble flux, and

$\alpha_j =$ removal rate coefficient for the j-th scrubbing mechanism (diffusion, inertia, sedimentation, condensation).

In the current model, the various removal mechanisms are treated as independent. Under this assumption, the total particle removal rate is calculated as the sum of the removal rates for the individual mechanisms, i.e.

$$\frac{dn}{dz} = -\sum_j \alpha_j\, n\,. \tag{3}$$

As discussed by Webb [13], the assumption of the independent removal mechanisms is valid for spherical bubbles, but can lead to a significant underprediction of the aerosol removal rate for highly deformed (ellipsoidal) bubbles when the vapour condensation rate is high. However, a more general treatment to account for this effect was not accounted for in the current version of the code.

Integration of Eq. (3) over the pool depth yields the number of aerosol particles with a given diameter exiting the pool upper surface. With this result, the DF for the given particle size is then evaluated through Eq. (1).

2.2. Aerosol Removal Rate Constants

The rate constants in Eqs. (2) and (3) for aerosol removed by diffusion, inertia, sedimentation, and condensation scrubbing mechanisms are defined in this section.

2.2.1. Brownian Diffusion

The rate constant for aerosol scrubbing by Brownian diffusion, as corrected in [6] for the case of ellipsoidal bubble deformations, is of the form:

$$\alpha_D = 6\sqrt{\frac{8\,\theta}{\pi\,U_B\,D_B^3}}\left[\frac{(E^2-1)\,F(E)}{1+\sqrt{4+2\,(E^2-1)}}\right], \tag{4}$$

where

$$\theta = \frac{K\,T_B\,C}{3\,\pi\,\mu_g\,d_a}, \tag{5}$$

$T_B =$ bubble bulk gas temperature (absolute),

$U_B =$ bubble rise velocity (as estimated by Peebles and Garber in [14]),

$D_B =$ average bubble diameter,

$K =$ Boltzman constant $= 1.3807x10^{-23}$ J/K,

$C =$ Cunningham slip correction,

$$C = 1 + \left(\frac{2\,\lambda}{d_a}\right)\left[1.257 + 0.4\exp(-0.55\;d_a/\lambda)\right], \tag{6}$$

$\lambda =$ mean free path of gas molecule,

$$\lambda = \frac{K\,T_B}{\sqrt{2}\,\pi\,d_g^2\,P_B}, \tag{7}$$

$d_a =$ aerosol particle diameter,

$d_g =$ effective gas molecule diameter,

$P_B =$ bubble absolute pressure,

$\mu_g =$ gas viscosity,

$E =$ bubble eccentricity, and

$$F(E) = \left[\frac{1.76\,E^2}{E^2-1} - \sqrt{2}\right]^{1/2} \left[\frac{E^2\ \tan^{-1}\left(\sqrt{E^2-1}\right)}{\sqrt{E^2-1}} - 1\right]^{-1/2}. \tag{8}$$

The eccentricity is defined as the ratio of the lengths of the major and minor axes of the bubble. For a spherical bubble, the eccentricity is therefore equal to unity. In the limit as $E \to 1$, Eq. (4) reduces to [6],

$$\alpha_D = 1.83\sqrt{\frac{8\,\theta}{\pi\,U_B\,D_B^3}}. \tag{9}$$

Note that the diffusion rate constant decreases as either the aerosol particle diameter or the gas bubble diameter increases.

2.2.2. Inertial Deposition

The rate constant for aerosol scrubbing by inertial deposition, including the effects of ellipsoidal bubble deformations, [6] is of the form:

$$\alpha_I = \frac{6\,U_B\,\tau\,G(E)}{D_B^2}, \tag{10}$$

where

$$\tau = \frac{\rho_a\,d_a^2\,C}{18\,\mu_g}, \tag{11}$$

$\rho_a =$ aerosol particle density, and

$$G(E) = \frac{E^{4/3}\left[(E^2-1)^2 + (E^2-1)^{3/2}\,(E^2-2)\ \tan^{-1}\left(\sqrt{E^2-1}\right)\right]}{\left[\sqrt{E^2-1} - E^2\ \tan^{-1}\left(\sqrt{E^2-1}\right)\right]^2}. \tag{12}$$

In the limit as $E \to 1$, Eq. (10) reduces to [6],

$$\alpha_I = \frac{18\,U_B\,\tau}{D_B^2}. \tag{13}$$

Note that the inertial deposition rate constant increases with increasing aerosol particle diameter and decreases with increasing gas bubble diameter.

2.2.3. Gravitational Sedimentation

The rate constant for gravitational sedimentation, modified for ellipsoidal bubble deformations, [6] is of the form:

$$\alpha_S = \frac{1.5\,g\,\tau\,E^{2/3}}{D_B\,U_B}, \tag{14}$$

where

$g =$ gravitational acceleration.

The sedimentation rate constant for the case of a spherical bubble is obtained by setting $E = 1$ in the above equation. From Eqs. (11) and (14), note that the sedimentation scrubbing rate increases with increasing aerosol particle diameter, and decreases with the average gas bubble diameter.

2.2.4. Condensation

The rate constant for aerosol scrubbing by vapour condensation at the gas/liquid interface is given through the expression [7],

$$\alpha_C = \frac{-6\,\dot{m}_V}{A_B\,D_B\,U_B\,\rho_g}, \tag{15}$$

where

$\dot{m}_V =$ steam generation rate at the gas/liquid interface,

$A_B =$ bubble surface area $= \pi\,{D_B}^2$, and

$\rho_g =$ bubble gas density.

The steam generation rate, $\dot{m}_V$, is taken to be positive if vaporization is occurring at the interface. As is evident from Eqs. (3) and (15), vapour condensation ($\dot{m}_V < 0$) acts to augment aerosol scrubbing. Conversely, the vapour flux from the interface during vaporization ($\dot{m}_V > 0$) acts to suppress scrubbing. To evaluate the vapour condensation rate, $\dot{m}_V$, would require utilizing a numerical algorithm to solve a coupled set of equations governing mass and energy transfer at the bubble gas/liquid interface. The IFR code instead utilizes a simplified approach to estimate aerosol scrubbing due to vapour condensation which is described in Section 2.3.

2.3. Model Simplifications

As described in the previous section, a numerical algorithm is required to solve the simultaneous set of equations governing aerosol transport through the sodium pool. The principal reason why a numerical solution is required is that the auxiliary equations governing the vapour condensation rate are highly non-linear. As an alternative approach, a simplified model for aerosol scrubbing due to vapour condensation was utilized in the IFR pool scrubbing code. With the condensation problem simplified, a numerical solution is no longer required to obtain approximate estimates of aerosol scrubbing in sodium including the effects of vapour condensation.

The following model for estimating the effect of vapour condensation on aerosol scrubbing was developed by Owcsarski et al. [15]. The basic assumptions underlying the model are: (i) the gas within the bubble attains thermal equilibrium with the pool in the immediate vicinity of the bubble entry point, and (ii) the aerosol particles are swept along with the condensing vapour so that the fraction of particles captured due to condensation is directly proportional to the fraction of gas that condenses. Given the first assumption, the initial condition on the bubble gas temperature becomes:

$$Temperature_{Bubble} = Temperature_{Pool}\,. \tag{16}$$

Given the second assumption, a condensation DF can be derived based on the fraction of inlet gas condensed, i.e. [15]

$$DF_C = \frac{1}{1-F} = \frac{X_{nc}^{eq}}{X_{nc}^{i}}, \tag{17}$$

where

$F =$ volume (mole) fraction of inlet gas condensed,

X_{nc}^{eq} = mole fraction of noncondensables in the bubble after thermal equilibrium is attained, and

X_{nc}^{i} = mole fraction of noncondensables in the inlet gas.

Note that Eq. (17) is independent of aerosol particle size.

If the additional assumption is made that the variation of hydrostatic pressure with submergence depth does not significantly affect the rate constants for diffusion, inertial deposition, and sedimentation removal processes, then simplified solutions may be obtained for these processes also. Under the assumption that the rate constants do not vary with submergence depth, then integration of Eq. (2) subject to the initial condition $n\,(z=0)=n_0$ yields,

$$n = n_0\, e^{-\alpha_j z}\,, \tag{18}$$

where

n_0 = number of aerosol particles in the bubble with diameter d_a at the injection point.

For a given aerosol particle diameter, d_a, DF's for the individual scrubbing processes are then found from Eqs. (1) and (18) as,

$$DF_D = e^{\alpha_D H_P}\,, \tag{19}$$

$$DF_I = e^{\alpha_I H_P}\,, \tag{20}$$

$$DF_S = e^{\alpha_S H_P}\,, \tag{21}$$

where

H_P = initial bubble submergence depth.

Note that the hydrostatic (i.e. bubble) pressure has been evaluated at the initial bubble submergence depth for the purposes of evaluating the rate constants in Eqs. (19) through (21). For a given particle diameter, a cumulative DF for all scrubbing processes is then found by combining Eqs. (17) and (19) through (21), which yields:

$$DF = \frac{X_{nc}^{eq}}{X_{nc}^{i}}\, e^{H_P\,(\alpha_D+\alpha_I+\alpha_S)} = DF_C\, DF_D\, DF_I\, DF_S\,. \tag{22}$$

Note that when condensation is included in the model, the rate constants for diffusion, inertia, and sedimentation scrubbing processes are evaluated based on the bubble diameter after vapour condensation has occurred (i.e., the bubble has thermally equilibrated with the surrounding coolant).

A detailed analysis of the mechanisms leading to bubble formation during fuel pin failure was not considered during development of the IFR pool scrubbing code. Rather, the assumption was made that the initial bubble size was limited by hydrodynamic [9] instability as gases and aerosols from failed fuel pin(s) exit the top of the fuel assembly region and enter into the overlying coolant pool. Thus, the initial bubble diameter is given through the expression [9],

$$D_B = \frac{\lambda}{2} = \pi \sqrt{\frac{3\,\sigma_l}{g\,(\rho_l - \rho_g)}}\,, \tag{23}$$

where

λ = Taylor wavelength,

σ_l = coolant surface tension, and

$\rho_l =$ coolant density.

Variations in bubble diameter from that predicted by Eq. (23) can be addressed through parametric calculations utilizing the IFR pool scrubbing code.

3. Analysis using the IFR Pool Scrubbing Code

The IFR pool scrubbing code was utilized to estimate the quantity of fission product aerosols that would be removed during two transient scenarios described in more detail in [4] and [16] in a pool-type SFR. The first scenario, referenced as PLOF+, is a protected loss-of-flow and loss-of-heat-sink transient coupled with degraded decay heat removal capability. The second scenario, referenced as UTOP+, is a large unprotected transient overpower coupled with degraded radial negative reactivity feedback. Both of these scenarios resulted in fuel pin cladding failures and the release of noble gas bubbles containing fission product aerosols into the primary sodium.

In the PLOF+ scenario, three fuel batches (referred to as Batch A, Batch B, and Batch C, see Table I for fuel batch parameters) experienced cladding failure and the IFR code was utilized to estimate the total DF for each fuel batch. The input parameters for the IFR code are provided in Table II. Note that the density of the aerosol particles was assumed to be equal to that of CsI and the diameter of the aerosol particles were assumed to be 0.1 μm. These assumptions are discussed later in this section. The code results for the three fuel batches are provided in Table III.

TABLE I: Fuel Batch Parameters

Parameter	**Batch A**	**Batch B**	**Batch C**
Number of Fuel Assemblies	60	60	60
Fuel Burnup (at%)	~2%	~5%	~10%
Internal Pin Gas Pressure (MPa)[1]	0.51	3.00	6.74

[1]At normal operating temperatures

TABLE II: PLOF+: Code Input Parameters

Parameter	**Batch A**	**Batch B**	**Batch C**
Sodium Pool Depth (m)	6.234	6.207	6.149
Sodium Pool Temperature (°C)	661	641	612
Cover Gas Pressure (Pa)	101325	101325	101325
Inlet Gas Temperature (°C)	754	741	719
Inlet Gas Pressure (Pa)	213102	213031	212910
Inlet Bubble Diameter (cm)	2.33	2.34	2.36
Aerosol Particle Density (kg/m^3)	4510	4510	4510
Aerosol Particle Diameter (μm)	0.1	0.1	0.1
Inlet Gas Vapour Content (mole %)			
Xenon	83.39	80.46	87.30
Krypton	3.47	5.31	6.05
Iodine	0.01	0.04	0.05
Rubidium	0.02	0.07	0.06
Cesium	0.72	3.40	3.19
Tellurium	0.00	0.00	0.00
Sodium	12.39	10.72	3.35

The overall DFs for the PLOF+ transient are relatively small due to several factors. First, the pool temperatures at the time of fuel pin failure are not significantly lower than the inlet gas temperatures. Therefore, very little sodium condensation occurs (which is evident in the condensation DF being approximately unity). The assumed small aerosol diameter (0.1 μm) results in both the inertial deposition DF and the gravitational DF being approximately unity.

No data were available to approximate the diameter of the aerosol particles, which has a significant impact of the overall DF. Also, a single aerosol particle density was assumed (4510 kg/m^3) instead of performing a calculation for each major species released. Instead, a sensitivity study was performed to demonstrate the effects of aerosol diameter and density on the total DF.

TABLE III: PLOF+: Decontamination Factor Results

Parameter	**Batch A**	**Batch B**	**Batch C**
Brownian Diffusion DF	2.7864	2.6374	2.4787
Inertial Deposition DF	1.1325	1.1227	1.1175
Gravitational Sedimentation DF	1.0169	1.0157	1.0153
Condensation DF	1.1317	1.1132	1.0303
Overall Total DF	**3.6310**	**3.3478**	**2.8972**

The results of the sensitivity study are provided in Figure 1 for fuel batch C. It is important to note that the total DF is not dependent on aerosol particle densities for aerosol particle diameters less than approximately 0.03 μm. In this region, Brownian diffusion is dominant, whereas inertial deposition and gravitational sedimentation become a greater factor at aerosol particle diameters greater than 0.03 μm. The results of the sensitivity study demonstrate the importance of aerosol particle diameter and density on the total DF.

The differences in total DF between the fuel batches of the PLOF+ scenario are due to the fuel in each batch experiencing cladding failure at different times during accident progression. As indicated in Table I, the internal pin pressure of each batch varies due to its burnup level (which depends on its residence time and location in the core). Fuel batch C fails first due to its high internal pin pressure (compared to fuel batches A and B). Because of the degraded decay heat removal capabilities of reactor, the temperature of the sodium pool continues to rise as the accident progresses. Therefore, the sodium pool temperature is lower when batch C fails than when batch B fails. The same is true of the pool conditions when batch B fails compared to when batch A fails. As the pool temperature increases the sodium thermally expands which increases the sodium pool depth above the core assemblies (see Table II). These differences lead to the overall DF being higher for batch A compared to batch B, and batch B compared to batch C.

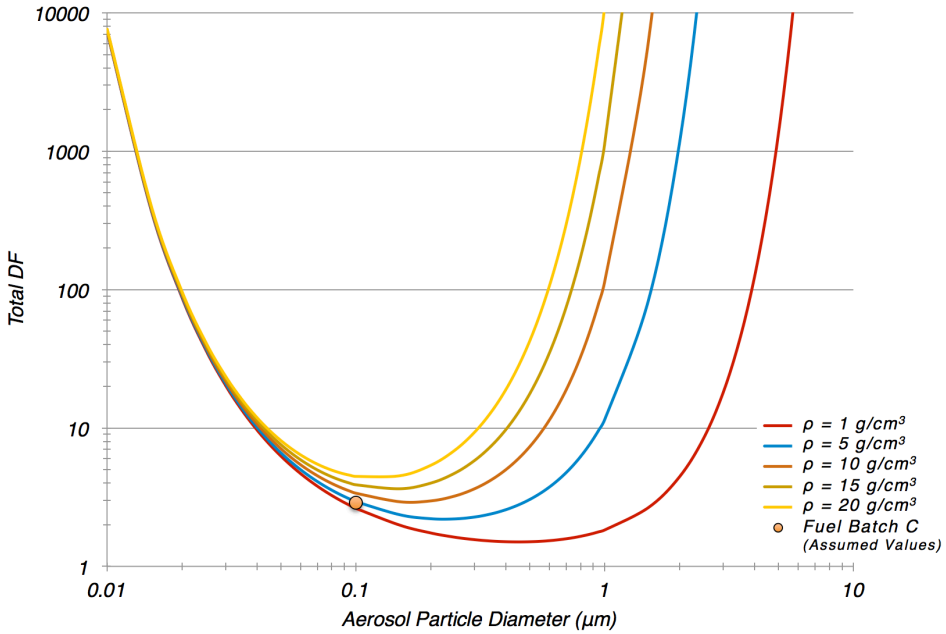

FIG. 1. PLOF+: Aerosol Diameter and Density Sensitivity Study (Fuel Batch C).

In the UTOP+ scenario, two fuel batches (referred to as Batch B and Batch C) experienced cladding failure and the IFR code was utilized to estimate the total DF for each fuel batch. The input parameters for the code are provided in Table IV. Note again that the density of the aerosol particles was assumed to be equal to that of CsI and the diameter of the aerosol particles was assumed to be 0.1 μm. The code results for the three fuel batches are provided in Table V.

The overall DFs of the UTOP+ transient are significantly higher than those of the PLOF+ transient. The largest DF for both fuel batches was the condensation DF. In this scenario, the inlet gas temperatures are much higher (1300°C and 1229°C) than the bulk sodium pool temperature (515°C). At these elevated temperatures, a significant fraction of the bond sodium in the pin is gaseous prior to pin failure, and condenses once it is released from the pin into the sodium pool.

As with the PLOF+ calculation, the assumed small aerosol diameter (0.1 μm) results in both the inertial deposition DF and the gravitational DF being approximately unity. A sensitivity study was performed with the UTOP+ results (fuel batch B) to demonstrate the effects of aerosol diameter and density on the total DF. The results of the sensitivity study are provided in Figure 2 for fuel batch B. The total DF for the UTOP+ scenario is higher than the PLOF+ for all aerosol densities. This is due to the condensation DF, which dominates in this scenario for all aerosol particle diameters and densities (as the condensation DF does not depend on either of these two parameters in the code). It is important to note that the total DF is not dependent on aerosol particle densities for aerosol particle diameters less than approximately 0.03 μm for the same reasons stated previously.

TABLE IV: UTOP+: Code Input Parameters

Parameter	**Batch B**	**Batch C**
Sodium Pool Depth (m)	6.045	6.045
Sodium Pool Temperature (°C)	515	515
Cover Gas Pressure (Pa)	101325	101325
Inlet Gas Temperature (°C)	1300	1229
Inlet Gas Pressure (Pa)	253374	252893
Inlet Bubble Diameter (cm)	2.40	2.40
Aerosol Particle Density (kg/m^3)	4510	4510
Aerosol Particle Diameter (μm)	0.1	0.1
Inlet Gas Vapour Content (mole %)		
Xenon	5.79	8.42
Krypton	0.40	0.59
Iodine	0.11	0.14
Rubidium	0.34	0.50
Cesium	4.58	6.83
Tellurium	0.00	0.00
Sodium	88.78	83.52

TABLE V: UTOP+: Decontamination Factor Results

Parameter	**Batch B**	**Batch C**
Brownian Diffusion DF	7.7053	5.3386
Inertial Deposition DF	1.1621	1.1382
Gravitational Sedimentation DF	1.0149	1.0137
Condensation DF	15.7217	10.6932
Overall Total DF	**142.8751**	**65.8660**

The differences in total DF between the fuel batches of the UTOP+ scenario are due to the inlet gas temperature and pressure of each fuel batch. Batch B has a higher gas temperature

and pressure than batch C, which increases the Brownian diffusion DF and the mole percentage of sodium in the vapour state in the pins prior to failure. When the pins fail, the sodium vapour condenses and as stated previously, it is assumed that aerosols particles are swept along with the condensing vapour. Since fuel batch B has more sodium vapour than batch C, more sodium is condensed and therefore more aerosols are scrubbed (i.e. the condensation DF of batch B is higher than batch C).

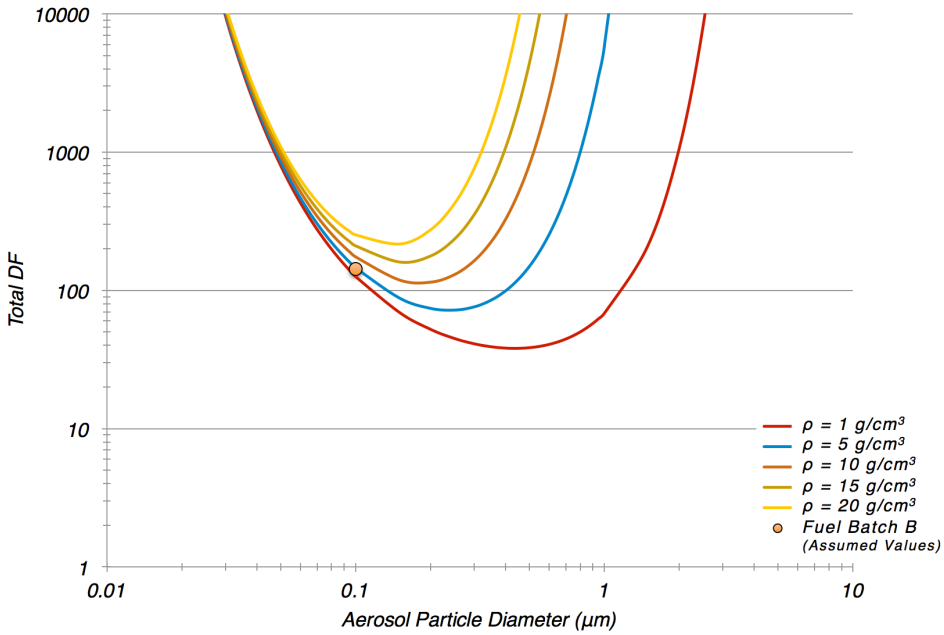

FIG. 2. UTOP+: Aerosol Diameter and Density Sensitivity Study (Fuel Batch B).

4. Summary

A fission product scrubbing in sodium pools computational code, developed as part of the IFR program, was utilized to perform part of a larger analysis to calculate a mechanistic source term for a metal-fuelled, pool-type SFR. The code accounts for fission product scrubbing via four mechanism: Brownian diffusion, inertial deposition, gravitational sedimentation, and sodium vapour condensation. The code does not address thermophoresis or diffusiophoresis scrubbing mechanisms. The results of the analyses using the code demonstrated the sensitivity of fission product scrubbing on aerosol particle diameter and density. The importance of condensation as a fission product scrubbing mechanism was also demonstrated by comparing the decontamination factors of the PLOF+ and UTOP+ scenarios.

5. Acknowledgements

Argonne National Laboratory's work was supported by the U.S. Department of Energy, Assistant Secretary for Nuclear Energy, Office of Nuclear Energy, under contract DE-AC02-06CH11357.

6. References

[1] U.S. NUCLEAR REGULATORY COMMISSION, “Issues Pertaining to the Advanced Reactor (PRISM, MHTGR, PIUS) and CANDU 3 Designs and their Relationship to Current Regulatory Requirements,” SECY-93-092, (1993).

[2] U.S. NUCLEAR REGULATORY COMMISSION, “Policy Issues Related to Licensing Non-Light Water Reactor Designs,” SECY-03-0047, (2003).

[3] U.S. NUCLEAR REGULATORY COMMISSION, “Second Status Paper on the Staff’s Proposed Regulatory Structure for New Plant Licensing and Update on Policy Issues Related to New Plant Licensing,” SECY-05-0006, (2005).

[4] GRABASKAS, D., BUCKNOR, M., JERDEN, J., BRUNETT, A.J., DENMAN, M., CLARK, A., DENNING, R.S., “Regulatory Technology Development Plan - Sodium Fast Reactor: Mechanistic Source Term Development - Trial Calculation,” Argonne National Laboratory, ANL-ART-49, (2016).

[5] FUCHS, N.A., The Mechanics of Aerosols, Pergamon Press, New York, NY (1964).

[6] POWERS, D.A., SPRUNG, J.L., “A Simplified Model of Aerosol Scrubbing by a Water pool Overlying Core Debris Interacting with Concrete,” NUREG/CR-5901, (1993).

[7] WASSEL, A.T., MILLS, A.F., BUGBY, D.C., “Analysis of Radionuclide Retention in Water Pools,” Nucl. Eng. Des. **90** (1985) 87.

[8] EPSTEIN, M., “Theory of Scrubbing of a Volatile Fission Product Vapor-Containing Gas Jet in a Water Pool,” ANS Winter Meeting Session on Thermal Hydraulics of Severe Accidents, 1:217, Washington, D.C. (1990).

[9] TAYLOR, G.I., “The Instability of Liquid Surfaces When Accelerated in a Direction Perpendicular to their Plane,” Proc. Royal Society **A201** (1950) 192.

[10] CASTLEMAN, Jr., A.W., “LMFBR Safety, I. Fission-Product Behavior in Sodium,” Nucl. Safety **11** (1970) 379.

[11] HAGA, K, et al., “Equilibrium and Nonequilibrium Partition Coefficients of Volatile Fission Products Between Liquid Sodium and the Gas Phase,” Nucl. Tech. **97** (1992) 17.

[12] TALBOT, L., et al., “Thermophoresis of Particles in a Heated Boundary Layer,” J. Fluid Mech. **101** (1980) 737.

[13] WEBB, S.W., “Coupling of Aerosol Removal Mechanisms in Rising Bubbles,” Trans. Am. Nucl. Soc. **52** (1986) 525.

[14] PEEBLES, F.N., GARBER, H.J., “Study on the Motion of Gas Bubbles in Liquids,” Chem. Eng. Prog. **44** (1953) 88.

[15] Owczarski, P.C., SCHRECK, R.I., POSTMA, A.K., “Technical Bases and User’s Manual for the Prototype of a Suppression Pool Aerosol Removal Code (SPARC),” NUREG/CR-3317, (1985).

[16] GRABASKAS, D., BUCKNOR, M. JERDEN, J., “A Mechanistic Source Term Calculation for a Metal Fuel Sodium Fast Reactor,” Proc. of the International Conference on Fast Reactors and Related Fuel Cycles: Next Generation Nuclear Systems for Sustainable Development (FR 17), Yekaterinburg, RU, (2017).